

Contents lists available at ScienceDirect

Journal of the Mechanics and Physics of Solids

journal homepage: www.elsevier.com/locate/jmps



Mechanistic mapping of random fields for stochastic finite element simulations of quasibrittle fracture

Josh Vievering, Jia-Liang Le*

Department of Civil, Environmental, and Geo- Engineering, University of Minnesota, United States of America

ARTICLE INFO

Keywords: Stochastic simulation Localization Mesh dependence Random fields Ouasibrittle materials Strain softening

ABSTRACT

Spurious mesh sensitivity is a major challenge in continuum finite element (FE) simulations of damage and fracture of quasibrittle structures. It has been shown that the existing localization limiters, which largely focus on energy regularization, are insufficient for addressing the issue of mesh sensitivity in stochastic analysis. In this study, we investigate the mathematical algorithm for mapping the continuous random fields of material properties onto the FE meshes. This is a fundamental problem in stochastic FE analysis, which has profound implications for the mesh sensitivity in the prediction of the statistics of failure behavior. We adopt a continuum damage constitutive model, and develop a mechanistic mapping method. The projection of the random fields of material properties onto the FE mesh is governed by the prevailing damage pattern of the element. The damage pattern of each finite element is determined based on the spatial distribution of the damage of its surrounding elements. Meanwhile, the prevailing damage pattern also dictates the energy regularization of the constitutive response of the finite element. The combination of energy regularization and mechanistic mapping method ensures that, for each time increment, the random tangential stiffness tensor of each finite element is calculated in accordance with the ongoing damage pattern. A direct consequence of the model is that, depending on the damage pattern, the statistics of the tangential stiffness tensor could vary with the mesh size. The model is applied to stochastic FE analysis of both notched and unnotched flexural specimens under different loading configurations, which exhibit different failure behaviors. The numerical analysis also considers different correlation lengths of the random fields of material properties. The simulation shows that, with the energy regularization scheme, the commonly used local mapping and local averaging methods could yield considerable mesh dependence of the statistics of the peak load capacity. The result also reveals the effect of correlation length on the spurious mesh dependence. By relating the mapping algorithm to the underlying damage pattern, the present model is able to mitigate the mesh sensitivity for different specimen geometries, loading configurations, and correlation lengths.

1. Introduction

Owing to the inherent uncertainties in both applied loads and structural resistance, reliability analysis plays a central role in the design of various engineering structures. Over the past two decades, significant attention has been paid to structures composed of quasibrittle materials, such as concrete, ceramics, fiber composites, rock, cold asphalt, etc. Major advances have been achieved

https://doi.org/10.1016/j.jmps.2024.105578

Corresponding author. E-mail address: jle@umn.edu (J.-L. Le).

in analytical modeling of quasibrittle structures. In a series of recent studies (Bazant and Pang, 2006; Bažant and Pang, 2007; Bažant et al., 2009; Le et al., 2011; Xu and Le, 2017; Bažant and Le, 2017), a finite weakest-link model was developed for the probability distribution of the nominal strength of quasibrittle structures failing at macrocrack initiation under controlled loads. The model was derived based on a statistical representation of the damage localization mechanism. Though this analytical model reveals some important features of strength distribution of quasibrittle structures including the size effect, it is unable to deal with structures of complex geometries. In subsequent studies, a fishnet model was proposed to capture both localized and diffused damage patterns (Luo and Bažant, 2017; Luo and Bažant, 2019; Xu et al., 2024). The fishnet model is analytically tractable for uniaxial tensile specimens with limited size range. Therefore, the stochastic finite element method (SFEM) remains the most versatile method for assessing the probability distribution of structural resistance.

The Monte Carlo simulation (MCS) is arguably the most widely used approach for SFEM. In general, MCS involves two steps: (1) mathematical representation of spatially distributed random material properties, and (2) numerical simulation of nonlinear structural response. The spatial randomness of the material properties can conveniently be described by random fields. Various mathematical models have been developed to numerically generate the random fields. The simplest case is the homogeneous Gaussian random fields, which can be simulated by the spectral representation method (Shinozuka and Deodatis, 1991, 1996) or the Karhunen–Loève expansion method (Karhunen, 1946; Spanos and Ghanem, 1989; Ghanem and Spanos, 1991). The non-Gaussian homogeneous fields can be handled using the correlation distortion methods involving a translation process (Yamazaki and Shinozuka, 1988; Shields et al., 2011; Field and Grigoriu, 2012) or the polynomial chaos expansion method (Sakamoto and Ghanem, 2002).

Numerical modeling of damage and failure of quasibrittle structures is complicated by the fact that quasibrittle materials often exhibit localization instability due to the strain-softening constitutive behavior. The localization instability leads to spurious mesh dependence in FE simulations (Bažant, 1976; Bazant and Cedolin, 1979; Pietruszczak and Mroz, 1981; Bažant and Oh, 1983; Bažant et al., 2021). Different regularization schemes have been proposed to address this fundamental issue. One class of the methods is anchored by the viewpoint that the constitutive law of the finite element represents the material-point behavior. To mitigate the mesh dependence, the concept of nonlocality is introduced into the constitutive relation in the form of either an integral model or gradient model (Bažant, 1984; Bažant and Pijaudier-Cabot, 1988; Peerlings et al., 1996). The other class of methods considers that the finite element represents a material element of finite size, and therefore the constitutive behavior of the finite element depends on the element size. The most well-known model in this class is the crack band model (Bažant and Oh, 1983; Bažant and Planas, 1998; Cervenka et al., 2005; Jirásek and Bauer, 2012), in which the post-peak region of the stress-strain curve is adjusted as a function of element size so as to preserve the fracture energy. The energy regularization scheme used in the crack band model considers the case of fully localized damage. However, in many cases, the failure process involves a transition from distributed to localized damage, which cannot readily be handled by the crack band model. In a recent study (Gorgogianni et al., 2020), a mechanism-based energy regularization model was proposed. In the model, the energy regularization is tied with the prevailing damage pattern, which may continuously evolve during the loading process. Consequently, the crack band model represents a limiting case of this general energy regularization scheme.

To complete the MCS scheme, the continuous random field of material properties needs to be mapped onto the FE mesh. Thus far in SFEM, two methods have widely been used: (1) direct local mapping (Haldar and Mahadevan, 2000; Vanmarcke, 2010) in which the random value of the constitutive parameter of finite element is taken directly from the underlying field at the centroid of the element, and (2) local averaging, in which the random constitutive parameter of the finite element is determined by taking the average of the corresponding random field over the domain of the finite element (Vanmarcke, 2010; Vanmarcke and Grigoriu, 1983; der Kiureghian and Ke, 1988; Deodatis, 1991). These two mapping methods are mathematically appealing because they lead to closed-form expressions for the probability distributions of constitutive properties for each Gauss point (Vanmarcke, 2010). However, from a physical viewpoint, they are questionable for the strength and fracture properties of quasibrittle materials. Consider the tensile strength of a finite element as an example. If the size of the localized damage zone is smaller than the element, the overall tensile strength of the finite element would be governed by the minimum of the tensile strengths of all potential damage zones in the element, which cannot be described by either direct local mapping or local averaging method. On the other hand, if the localized damage zone occupies the entire finite element, which represents a distributed damage pattern, the tensile strength of the element can be taken as the average of the random tensile strengths of the material inside the entire element. Therefore, for quasibrittle materials, the mapping method of random fields of material properties and the consequent probability distributions of the constitutive properties of finite element are strongly affected by the damage pattern.

Recent studies have discovered that, for SFEM, the energy regularization of the constitutive relationship alone is insufficient for mitigating the spurious mesh dependence in the prediction of the statistics of structural response (Le and Eliáš, 2016; Gorgogianni et al., 2022). Special care is needed for the formulation of the probability distribution functions of constitutive properties. These studies considered the FE mesh to be significantly larger than the correlation length of the random fields of material properties. Therefore, the random constitutive properties of each finite element can be sampled independently from their cumulative distribution functions (cdfs). The cdfs of constitutive properties were formulated analytically based on the prevailing damage pattern of the finite element. The model predicts that the cdfs of some constitutive properties would depend on the mesh size. It was found that this mechanism-based modeling of cdfs of constitutive properties plays an essential role in mitigating the mesh dependence in SFEM (Le and Eliáš, 2016; Gorgogianni et al., 2022).

Though the aforementioned model elucidates the critical importance of relating the cdfs of constitutive properties to the damage pattern (Le and Eliáš, 2016; Gorgogianni et al., 2022), it ignores the spatial correlation of the random material properties by placing some restrictions on the FE mesh size in relation to the correlation length and the width of the fracture process zone (FPZ). These restrictions may not be fulfilled in some general scenarios. For example, one may choose an FE mesh that is not much larger than

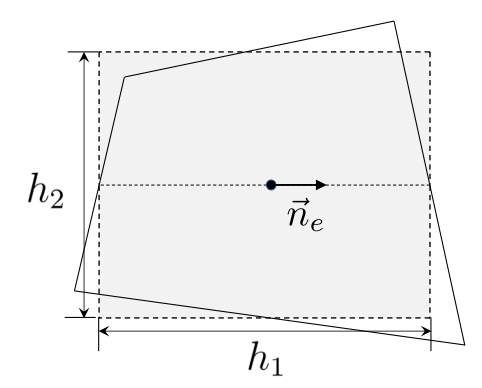


Fig. 1. Definition of mesh size of a quadrilateral finite element.

the correlation length. To remove these restrictions, we would need to directly use the random fields of material properties in SFEM. Based on the findings of the aforementioned studies, it has transpired that the mapping algorithm of the random fields of material properties needs to be devised according to the damage pattern of the finite element. The focus of this study is to develop such a mechanism-based mapping method, and to examine its performance in stochastic FE simulations of quasibrittle fracture.

2. Constitutive model

This study adopts a recently developed isotropic damage model with a general energy regularization scheme for tension-dominant failure (Gorgogianni et al., 2020, 2022). The section provides a brief review of this model. The stress–strain relationship is written as

$$\sigma = f(\omega)C : \epsilon \tag{1}$$

where C is the elastic stiffness tensor, ω is a scalar damage variable taking a value from 0 (virgin state) to 1 (fully damaged state), ε is the infinitesimal strain tensor, and $f(\omega)$ is a damage function, which characterizes the stiffness degradation. Function $f(\omega)$ decreases monotonically from 1 to 0 as ω increases.

In FE models, the constitutive relationship provides a smeared representation of the mechanical behavior of the element. For quasibrittle materials, the mechanical response of the finite element is generally inhomogenous. It is of critical importance to ensure that the constitutive model of the finite element would predict the correct energy dissipation regardless of the subjective choice of the mesh size. Since we focus on the tension-dominant failure and ignore the plasticity, it is natural to link the energy dissipated due to damage to the mode I fracture energy.

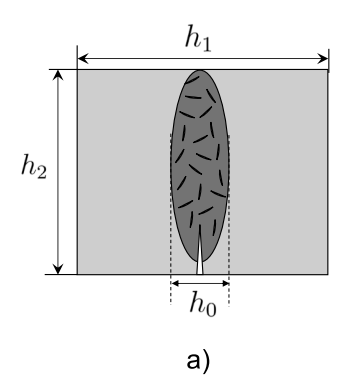
To this end, we postulate a free energy function $Y(\omega,\epsilon)$, where the energy release (per unit thickness) of the finite element due to an increment amount of damage $\delta\omega$ is equal to $A_e\delta Y$, where A_e = area of finite element. This amount of energy is expended for crack propagation inside the element. For tension-dominant failure, it is reasonable to consider that cracks will form in the direction perpendicular to the maximum principal strain direction denoted by a unit vector \vec{n}_g . Consider a quadrilateral element, and let h_1 be the width of the element passing through the centroid of the element in the direction of a principal vector \vec{n}_e (Fig. 1). Before damage occurs, \vec{n}_e is equal to \vec{n}_g , which may change during the loading process. After damage initiates, \vec{n}_e is set to be \vec{n}_g measured at the onset of damage. In other words, we consider that the direction of crack propagation within the element is fixed, i.e. a fixed crack model. Nevertheless, as will be discussed later, the size of the damage band may change after damage initiation. Once h_1 is determined, we define element size h_2 in the orthogonal direction such that $A_e = h_1 h_2$.

For a damage increment $\delta\omega$, the total new surface area (per unit thickness) created is given by $n_bh_2\delta\omega$, where n_b is the number of cracks propagating together in the element. Evidently, the damage parameter ω is defined such that the total length of each crack is equal to ωh_2 . This is different from the classical continuum damage mechanics model, where ω directly characterizes the stiffness degradation (Kachanov, 1986). For quasibrittle materials, a FPZ forms at the tip of each macroscopic crack. The FPZ contains a large number of microcracks. The global fracture energy is related to the total energy dissipation inside the FPZ. The balance between the energy released by damage and the energy expended for crack propagation can be written as

$$\frac{\partial Y}{\partial \omega} + \frac{n_b \widetilde{G}_f}{h_1} = 0 \tag{2}$$

where \widetilde{G}_f = average value of fracture energies of n_b FPZs. Following Gorgogianni et al. (2022), we consider the following free energy function

$$Y = \frac{1}{2}f(\omega)\widetilde{E}\bar{\epsilon}^2 \tag{3}$$



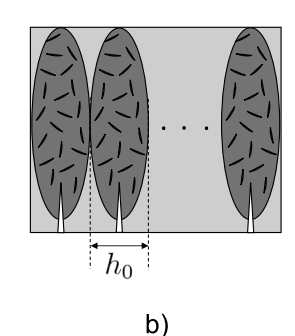


Fig. 2. Two damage patterns of a material element under uniaxial tension: (a) fully localized damage, and (b) distributed damage.

where \widetilde{E} is the average Young's modulus of the element, and $\overline{\epsilon} = \sqrt{\sum_{i=1}^{3} \langle \epsilon_i \rangle^2}$ ($\epsilon_i = \text{principal strains}, \langle \cdot \rangle = \text{Macaulay bracket}$) (Mazars, 1984). Now consider the case of uniaxial tension. The total energy required to completely damage the element is given by

$$\mathcal{E} = h_1 h_2 \int_0^\infty \sigma d\epsilon = -h_1 h_2 \widetilde{E} \int_0^1 \frac{1}{2} \epsilon^2 \frac{df(\omega)}{d\omega} d\omega \tag{4}$$

By substituting Eqs. (2) and (3) into (4), we have $\mathcal{E} = n_b h_2 \widetilde{G}_f$. This indicates that, regardless of the element size, the energy dissipation calculated from the stress-strain relationship matches the energy expended in crack propagation.

Eq. (2) gives some insights into the constitutive response of the finite element. For the case of purely localized damage, there is only one macrocrack propagating, i.e. $n_b = 1$ (Fig. 2a). It is clear from Eq. (2) that the constitutive relationship depends on the element size h_1 . In the other limiting case, where the element experiences fully distributed damage (Fig. 2b), we have $n_b = h_1/h_0$, where $h_0 = \text{FPZ}$ width, a material characteristic length. In this scenario, Eq. (2) indicates that the constitutive relationship is independent of element size because the element experiences a homogeneous deformation.

The number of active macrocracks, n_b , is determined by the level of damage localization. It has been suggested that the localization level of each finite element can be quantified based on the local damage patterns of the two adjacent elements aligned most closely with principal vector \vec{n}_e (Le and Eliáš, 2016). For element i, the following localization parameter was recently proposed (Gorgogianni et al., 2022):

$$\chi_1 = \left\langle 1 - \frac{\hat{\omega}_m + \hat{\omega}_n}{2\hat{\omega}_i} \right\rangle^{1/2} \tag{5}$$

where $\hat{\omega}_k$ (k=i,m,n) denotes the representative damage level of element k. To mitigate the influence of stochasticity in local stress and strain fields on the determination of the overall damage pattern, the representative damage level of element k is determined as a weighted average of the damage values of the element itself and the two adjacent elements that are aligned closest to the direction of the principal vector of element k: $\hat{\omega}_k = \alpha_\omega \bar{\omega}_k + 0.5(1 - \alpha_\omega) \left(\bar{\omega}_{k-1} + \bar{\omega}_{k+1} \right)$, where $\bar{\omega}_r(r=k, k-1, k+1) =$ the damage level of element r averaged over all Gauss points of the finite element. Following Gorgogianni et al. (2022), we choose $\alpha_\omega = 0.5$.

Based on Eq. (5), the localization parameter χ_1 takes the minimum value of 0 for the case of purely diffused damage. In the case of fully localized damage, χ_1 attains its maximum value $\chi_m = \left\langle 1.5 - 0.5\alpha_\omega^{-1} \right\rangle^{1/2}$. For each finite element, the number of active FPZs is related to its localization parameter by

$$n_b = 1 + \left(\frac{h_1}{h_0} - 1\right) \left\{ 1 - \left[\frac{\langle \chi_1 - \chi_{t1} \rangle}{\chi_m - \chi_{t1}}\right]^{\kappa} \right\}$$
 (6)

where κ and χ_{t1} are constants. χ_{t1} determines the threshold value of χ_1 below which the element is deemed to experience a fully diffused damage pattern. κ describes the transitional behavior between the fully diffused damage case and the fully localized damage case in terms of χ_1 .

The constitutive model is completed by prescribing the form of damage function $f(\omega)$, which determines the nonlinear stress-strain behavior. In this study we use the following $f(\omega)$ function, which yields an exponential softening behavior under uniaxial tension (Wu and Nguyen, 2018):

$$f(\omega) = \frac{(1-\omega)^2}{(1-\omega)^2 + \eta\omega(1-\omega/2)}$$
(7)

where:
$$\eta = \frac{2n_b \widetilde{E} \widetilde{G}_f}{h_1 \widetilde{f}_i^2}$$
 (8)

Fig. 3 shows a set of uniaxial tensile stress—strain curves for different finite element sizes for the case of full damage localization. It is seen that the post-peak response varies with the element size in order to preserve the fracture energy. In a general case, the damage pattern of a finite element could evolve during the loading process. During each time step, the tangential stiffness of the element is calculated based on the current damage pattern, for which the proper energy regularization requirement is satisfied.

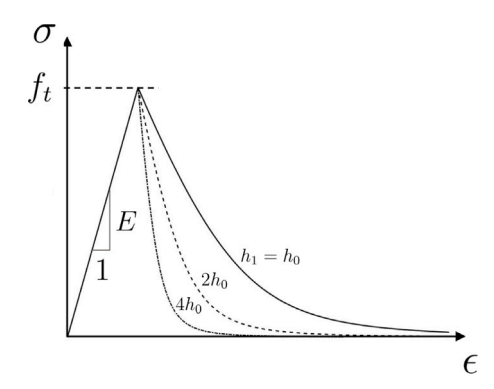


Fig. 3. Uniaxial tensile stress-strain curves for different finite element sizes for the case of fully localized damage.

3. Modeling of random constitutive properties

3.1. Generation of random fields of material properties

The parameters of the constitutive model represent the apparent properties of the finite element. They should be distinguished from the actual material properties, which are defined for a material point in the context of continuum mechanics. For deterministic analysis, the material-point properties are considered to be the same as the properties of the finite element. However, in stochastic analysis both the mean and higher order statistical moments of the constitutive properties of the finite element could differ considerably from those of material-point properties.

Due to the heterogeneous nature of quasibrittle materials, the material-point properties are expected to exhibit a considerable degree of spatial variability, which can mathematically be described by random fields. Here we consider these random fields to be homogeneous and statistically independent. For material property H, the corresponding random field can be written by

$$H(\mathbf{x}) = \bar{H} + \delta H(\mathbf{x}) \tag{9}$$

where \bar{H} is the mean value of H, and $\delta H(x)$ represents the spatial variation of H, which is described by a zero-mean homogeneous random field. $\delta H(x)$ can be generated by using the power spectral density method (Shinozuka and Deodatis, 1991, 1996). If material property H at a local point can be described by a Gaussian cdf, the corresponding random field $\delta H(x)$ in 2D can be expressed by Shinozuka and Deodatis (1996)

$$\delta H(x_1, x_2) = \sqrt{2} \sum_{n_1=0}^{N_1-1} \sum_{n_2=0}^{N_2-1} \left\{ A_{n_1 n_2} \cos \left(\kappa_{1 n_1} x_1 + \kappa_{2 n_2} x_2 + \boldsymbol{\varPhi}_{n_1 n_2}^{(1)} \right) + \widetilde{A}_{n_1 n_2} \cos \left(\kappa_{1 n_1} x_1 - \kappa_{2 n_2} x_2 + \boldsymbol{\varPhi}_{n_1 n_2}^{(2)} \right) \right\}$$
 (10)

where $\Phi_{n_1n_2}^{(1)}$ and $\Phi_{n_1n_2}^{(2)}$ are two sets of independent random phase angles uniformly distributed over the interval $[0, 2\pi]$, $A_{n_1n_2} = \sqrt{2S(\kappa_{1n_1}, \kappa_{2n_2})\Delta\kappa_1\Delta\kappa_2}$, $\widetilde{A}_{n_1n_2} = \sqrt{2S(\kappa_{1n_1}, -\kappa_{2n_2})\Delta\kappa_1\Delta\kappa_2}$, $\kappa_{1n_1} = n_1\Delta\kappa_1$, $\kappa_{2n_2} = n_2\Delta\kappa_2$, $\Delta\kappa_1 = \kappa_{1u}/N_1$, $\Delta\kappa_2 = \kappa_{2u}/N_2$, and κ_{1u}, κ_{2u} are the upper cut-off wave numbers along the x_1 - and x_2 - axes in the space domain, respectively. $S(\kappa_1, \kappa_2)$ is the power spectral density function (PSDF) of the random field, which is related to the covariance function $R(\tau_1, \tau_2)$ of $\delta H(x)$ through the Wiener-Khintchine theorem (Vanmarcke, 2010):

$$S(\kappa_1, \kappa_2) = \frac{1}{(2\pi)^2} \int_{-\infty}^{\infty} \int_{-\infty}^{\infty} R(\tau_1, \tau_2) \exp[-i(\kappa_1 \tau_1 + \kappa_2 \tau_2)] d\tau_1 d\tau_2$$

$$\tag{11}$$

When N_1, N_2 are sufficiently large, the cdf of δH at a given point approaches a standard Gaussian distribution due to the Central Limit Theorem. The upper cut-off wave numbers, κ_{1u} and κ_{2u} , are chosen so that the value of integral $\int_{-\kappa_{2u}}^{\kappa_{1u}} S(\kappa_1, \kappa_2) \mathrm{d}\kappa_1 \mathrm{d}\kappa_2$ converges with a relative tolerance of 1%. In this study, $\delta H(x_1, x_2)$ is simulated by using the Fast Fourier Transform (Shinozuka and Deodatis, 1996). It should be pointed out that, when generating the stochastic field, the spatial grid sizes, Δx_1 and Δx_2 , need to be sufficiently small ($\Delta x_i \leq \pi/\kappa_{ui}$ (i=1,2)) so as to avoid aliasing (Bracewell, 1999).

If $\delta H(x_1,x_2)$ is non-Gaussian, we first generate a Gaussian random field $\delta H_G(x_1,x_2)$ using Eq. (10) and then transform it to the target non-Gaussian field by

$$\delta H(x_1, x_2) = F_H^{-1}(F_G(\delta H_G(x_1, x_2))) \tag{12}$$

where $F_H(h)$ is the cdf of δH at a given point, $F_G(h)$ is a zero-mean Gaussian cdf with its standard deviation δ_h equal to the standard deviation of δH . To generate the equivalent Gaussian field $\delta H_G(x_1,x_2)$, we also need to know its covariance function $R_G(\tau_1,\tau_2)$. It is noted that $R_G(\tau_1,\tau_2)$ is related to the covariance function of $\delta H(x_1,x_2)$ by Grigoriu (1995)

$$R(\tau_1, \tau_2) = \int_{-\infty}^{+\infty} \int_{-\infty}^{+\infty} F_H^{-1}(F_G(x_1)) F_H^{-1}(F_G(x_2)) \phi(x_1, x_2; \rho(\tau_1, \tau_2)) dx_1 dx_2$$
(13)

where:

$$\phi(x_1, x_2; \rho(\tau_1, \tau_2)) = \frac{1}{2\pi\delta_h^2 \sqrt{1 - \rho^2(\tau_1, \tau_2)}} \exp\left\{-\frac{x_1^2 + x_2^2 - 2\rho(\tau_1, \tau_2)x_1x_2}{2\delta_h^2 [1 - \rho^2(\tau_1, \tau_2)]}\right\}$$
(14)

and $\rho(\tau_1, \tau_2) = R_G(\tau_1, \tau_2)/\delta_h^2$. Since the covariance function of $\delta H(x_1, x_2)$ is given, we would need to determine the corresponding covariance function $R_G(\tau_1, \tau_2)$ of the equivalent Gaussian field $\delta H_G(x_1, x_2)$ that satisfies Eq. (13).

As indicated by Eq. (10), the mathematical representation of the Gaussian field relies on the PSDF of the field. It has been shown that the PSDF, $S_G(\kappa_1, \kappa_2)$, of the equivalent Gaussian field can be approximated through an iterative correlation distortion technique (Yamazaki and Shinozuka, 1988). For the *i*th iteration, the equivalent Gaussian field $\delta H^i_G(x_1, x_2)$ is generated by using Eq. (10). Through Eq. (12), we can calculate the corresponding target random field $\delta H^i(x_1, x_2)$ as well as its PSDF $S^i_{NG}(\kappa)$. The PSDF of the equivalent Gaussian field will then be updated by (Yamazaki and Shinozuka, 1988)

$$S_G^{i+1}(\kappa_1, \kappa_2) = \frac{S_G^i(\kappa_1, \kappa_2)}{S_{NG}^i(\kappa_1, \kappa_2)} S_{NG}^T(\kappa_1, \kappa_2)$$
(15)

where $S_{NG}^T(\kappa_1, \kappa_2)$ is the target PSDF for the non-Gaussian field $\delta H(x_1, x_2)$ and $S_G^i(\kappa_1, \kappa_2)$ is the PSDF of the equivalent Gaussian field at the current step. The iterative process begins by setting the PSDF of $\delta H_G(x_1, x_2)$ equal to $S_{NG}^T(\kappa_1, \kappa_2)$ (Yamazaki and Shinozuka, 1988). The iteration is terminated when $S_{NG}^i(\kappa_1, \kappa_2)$ is approximately equal to $S_{NG}^i(\kappa_1, \kappa_2)$ within a small tolerance.

In the present study, we consider that the material properties are statistically independent of each other since the primary objective here is to examine the performance of the mapping method. In real engineering applications, different material properties could exhibit cross-correlation features, which can be included in the present model by generating cross-correlated random fields of material properties using the spectral representation method, which involves factorization of the cross-spectral matrix (Vio et al., 2002), or the Karhunen–Loéve expansion method (Vořechovský, 2008; Wu et al., 2023).

3.2. Mapping of random fields onto FE mesh

The random fields of material properties serve as an objective input to the FE model. Since the grid size used for generating the random fields of material properties is very different (usually much smaller) as compared to the FE mesh size, the essential question here is how to extract the constitutive properties of each finite element from a given realization of random fields of material properties. The existing mapping methods, such as local mapping and local averaging methods, were proposed from a mathematical viewpoint. Little attention has been paid to how to tie the mapping methods with the physical behavior of the material. Recent studies have shown that, for stochastic FE analysis of quasibrittle fracture, the cdfs of the constitutive properties of the FE mesh are strongly dependent on the damage pattern (Le and Eliáš, 2016; Gorgogianni et al., 2022). Therefore, it is naturally expected that the mapping of random fields of material properties to the FE mesh needs to be directly related to the damage pattern of the finite element. Since the damage pattern may evolve during the loading process, the mapping method would need to be adjusted accordingly. In this section, we will introduce a new mapping method which ensures that the statistics of the constitutive properties of the finite element are determined according to the prevailing damage pattern.

Consider a finite element of size $h_1 \times h_2$ that lays over a random field H(x), which is generated using a grid of size Δx that is aligned with the global coordinate system of the specimen. Since the element is rotated to its principal direction \vec{n}_e , we rotate the underlying random fields accordingly so as to align with the element orientation (Fig. 4). Since the grid size is small, the values of random properties of the rotated grid of the random fields can be determined by bilinear interpolation. For a given realization of H(x), the random values of H(x) of all the grids covered by the finite element are stored in a matrix h of size $p \times q$, where p, q = n numbers of grids along h_2 and h_1 directions, respectively. The present constitutive model involves three constitutive constants: Young modulus \tilde{E} , tensile strength \tilde{f}_t , and mode I fracture energy \tilde{G}_f , which are apparent properties of the finite element. The corresponding material-point properties are denoted by E, f_t , and G_f , which are represented by the random fields.

The Young modulus of the finite element is taken as the average of the Young moduli of all the grids inside the finite element, i.e.

$$\widetilde{E} = \frac{1}{na} a h_E b^T \tag{16}$$

where a is a $1 \times p$ array of ones, b is a $1 \times q$ array of ones, h_E is the matrix containing the values of the random field of Young modulus, and the superscript T denotes transpose of the matrix. Note that taking the arithmetic mean of the underlying field E(x) over the entire finite element is one limiting approach of handling the spatial varying Young modulus. The other limiting approach is to use the harmonic mean. The actual behavior would lie in between. Nevertheless, our preliminary simulation shows that, because of a large number of sampling points within each finite element, the statistics of arithmetic mean and harmonic mean are very close to each other. For the sake of convenience, we use the arithmetic mean in this study.

By contrast, the mappings of tensile strength $\widetilde{f_i}$ and fracture energy \widetilde{G}_f need to be tied to the damage pattern. As discussed in Section 2, the essential parameter for energy regularization is the number n_b of active macrocracks in the finite element, which can also be understood as the damage band width h_b . Based on Eq. (6), h_b can be expressed by

$$h_b = n_b h_0 = h_0 + (h_1 - h_0) \left\{ 1 - \left[\frac{\langle \chi_1 - \chi_{t1} \rangle}{\chi_m - \chi_{t1}} \right]^{\kappa} \right\}$$
 (17)

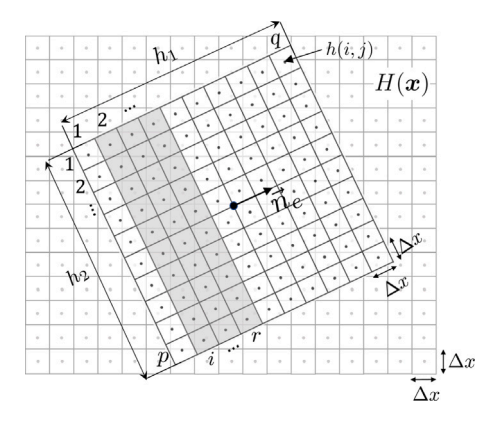


Fig. 4. A finite element laying over a random field of material property.

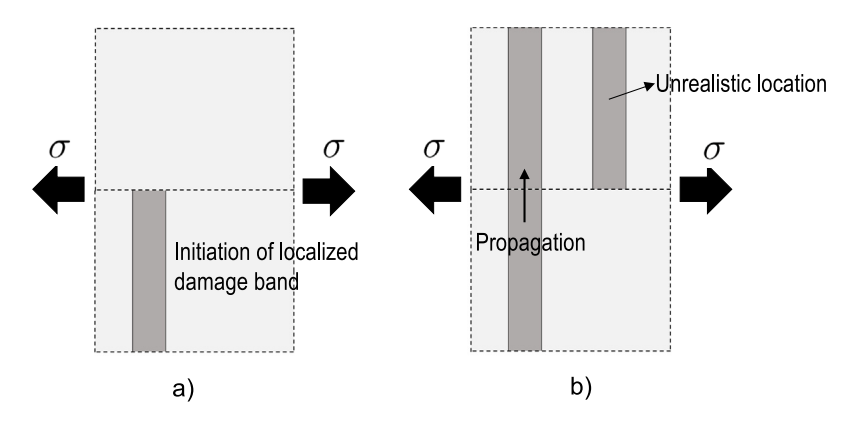


Fig. 5. Schematics of (a) initiation of localized damage, and (b) propagation of localized damage.

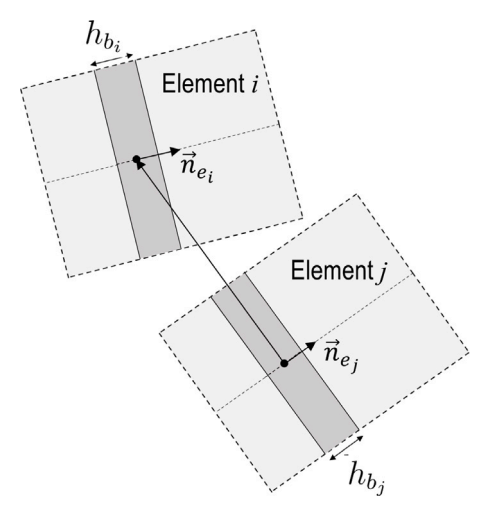


Fig. 6. Identification of the location of a propagating localized damage band.

In deterministic analysis, h_b is used only to determine the energy dissipation of the finite element, which does not affect the input constitutive properties. This is not the case for stochastic analysis. When we introduce the spatial randomness of material properties, the location of the damage band is intrinsically random, which has important implications for the cdfs of constitutive properties of the finite element.

To discuss the mapping of $f_t(\mathbf{x})$ and $G_f(\mathbf{x})$, we first need to distinguish two scenarios of localized damage: (1) a localized damage band initiates inside the element (Fig. 5a), and (2) the localized damage band forms inside the element due to the propagation of

localized damage from an adjacent element (Fig. 5b). These two scenarios have the same energy regularization since the total energy dissipation of the element is equal to the energy expended to form a single damage band. However, the treatments of statistics of tensile strength \tilde{f}_t and fracture energy \tilde{G}_f for these two cases are different. In the first scenario, the location of the damage band is intrinsically random, whereas in the second scenario the location of damage band of the current element is determined by the damage band previously formed in the adjacent element. To differentiate these two cases, for finite element i, we propose the following parameter

$$\chi_2 = \max_j \left[\chi_{1j} \left(1 - \left| \vec{n}_e \cdot \vec{v}_{ij} \right| \right) \right] \tag{18}$$

where \vec{v}_{ij} is a unit vector in the direction from the centroid of element i to that of its adjacent element j (Fig. 6), and χ_{1i} is the value of χ_1 of element j given by Eq. (5). It is evident that parameter χ_2 takes its maximum value, χ_m , when an adjacent element exhibits fully localized damage and this element is perfectly aligned with the direction of the damage band of the current element i. Therefore, it is reasonable to consider that, when χ_2 exceeds a threshold value χ_{12} , the damage in element i would be fully localized (i.e. $h_b = h_0$) and this damage is due to the propagation of a localized damage band in one of its surrounding elements. When χ_2 is smaller than χ_{12} , the damage in element i is determined solely by parameter χ_1 . By introducing χ_2 , we can formulate the following mapping methods for \widetilde{f}_i and \widetilde{G}_f for the aforementioned two scenarios:

• Case I: $\chi_2 \leq \chi_{t2}$:

In this case, we consider that the damage band forms at the location where the average tensile strength of the band is the minimum. This is a simplification because the formation of the damage band may occur somewhere in the post-peak regime of the response of the finite element. A precise determination of the onset of damage band is a daunting task. Nevertheless, it should be pointed out that, even if the onset of damage band occurs in the post-peak regime, it would be close to the peak stress. Therefore, the present simplification at the element level is reasonable, and has a minimal effect on the global behavior of the structure.

Based on the foregoing discussion, the apparent tensile strength is equal to the minimum average tensile strength of all the potential damage bands in the element. The average tensile strength of one band starting at grid i in h_1 direction is given by

$$f_t^i = \frac{1}{pn_d} a \mathbf{h}_{f_t} \mathbf{c}_i^T \tag{19}$$

where

$$c_i = \begin{bmatrix} 1 & \cdot & i & \cdot & \cdot & r & \cdot & \cdot & q \\ 0 & 0 & 1 & 1 & 1 & 1 & 0 & 0 & 0 \end{bmatrix}$$
 (20)

 h_{f_i} is the matrix containing the values of the random field of material tensile strength, $r = i + n_d - 1$, and $n_d = h_b/\Delta x$. The apparent tensile strength of the finite element is then given by

$$\widetilde{f}_t = \min_{i \in [1, q_-]} \left[f_t^i \right] \tag{21}$$

where $q_m = q - n_d + 1$. It should be mentioned that, since f_i^i generally exhibit a spatial correlation structure, the exact expression of the cdf of \tilde{f}_t is not possible. One may obtain approximate solutions under certain assumptions (Xu and Le, 2017; Le, 2020), which could be too restrictive for the present study. Furthermore, the spatial correlation of f_t among different elements is difficult to determine because each element may have a different direction of the principal vector \vec{n}_e . Therefore, in this study we numerically determine the random tensile strength of the finite element for each realization (Eq. (21)).

Let i^* denote the grid number in h_1 direction of the damage band location (i.e. f_t^i is minimum). The apparent fracture energy of the finite element is the average fracture energy of the damage band, i.e.

$$\widetilde{G}_f = \frac{1}{pn_d} a \mathbf{h}_{G_f} \mathbf{c}_{i^*}^T \tag{22}$$

where \mathbf{h}_{G_f} is the matrix containing the values of the random field of fracture energy.

In this case, the damage band in the current element is formed as a result of the propagation of the localized damage band from the adjacent element. Consider that the adjacent element j experiences localized damage, where the centroid of this damage band is denoted by \vec{x}_{b_i} . The centroid of the damage band in the current element i is located at the intersection between the line emanating from the centroid \vec{x}_{b_j} in the direction of the principal vector \vec{n}_e^j of element j and the centerline of the current element in the direction of its principal vector (Fig. 6).

Once the location of the damage band is determined, the apparent tensile strength and fracture energy of the current element are computed as an average over this particular damage band, i.e.:

$$\widetilde{f}_t = \frac{1}{p n_d} a h_{f_t} c_p^T \tag{23}$$

$$\widetilde{G}_f = \frac{1}{pn_d} \mathbf{a} \mathbf{h}_{G_f} \mathbf{c}_p^T \tag{24}$$

where subscript p refers to the value of $i \in [1, q]$ corresponding to the damage band location in the current element based on damage propagation from an adjacent element.

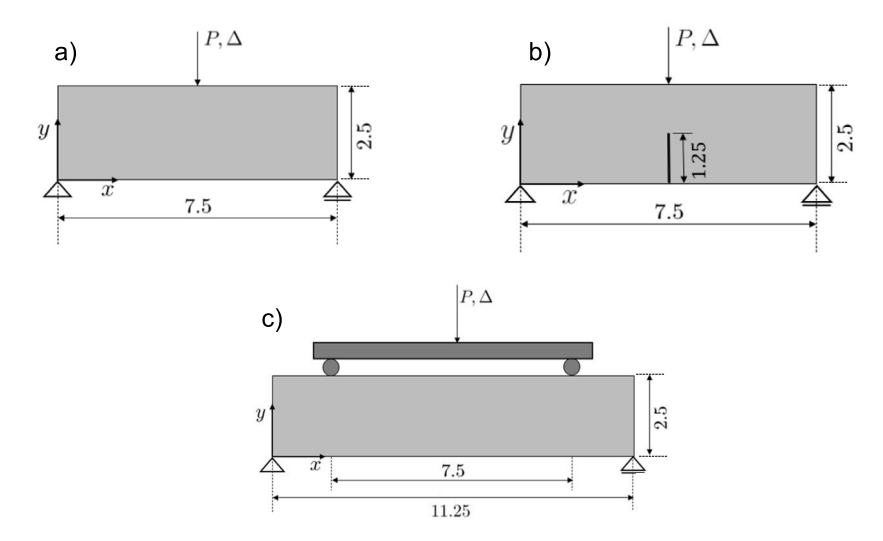


Fig. 7. Flexural specimens considered in the numerical study (all dimensions are in mm): (a) unnotched three-point bend beam, (b) notched three-point bend beam, and (c) unnotched four-point bend beam.

In addition to the aforementioned mapping method for $\widetilde{f_t}$ and \widetilde{G}_f , we need to specify the initial mapping of these two quantities before any damage occurs. In the initial elastic regime, the deformation inside the element is homogeneous, and we calculate the apparent tensile strength and fracture energy by averaging the corresponding random fields that are covered by the finite element. This treatment applies to the scenarios where the specimen initially exhibits a diffused damage, but is not accurate for specimens experiencing a localized damage immediately after the elastic response. However, it is expected that the consequence for the prediction of the global behavior would be negligible since this error only occurs in one time step. During the subsequent time step, the localization parameter would indicate the localized damage pattern, and the mapping method for $\widetilde{f_t}$ and \widetilde{G}_f would be adjusted accordingly.

It is clear that the proposed mapping of the random fields of tensile strength and fracture energy is intimately related to the damage pattern. The present model ensures that, during each time increment, the sampling of the random constitutive properties of the finite element and consequently the calculation of the random tangential stiffness tensor are consistent with the prevailing damage pattern. This is the key feature of the present model, as compared to the existing mapping method for the random fields in which a fixed mapping algorithm is used regardless of the evolution of damage pattern. It should also be pointed out that, based on Eq. (21), the statistics of the apparent tensile strength, and consequently the tangential stiffness of the finite element could strongly depend on the mesh size. This size dependence arises from the fact that each finite element represents a material element of finite size. Due to damage localization, the element experiences an inhomogeneous deformation field, which is characterized by length parameter h_b . Consequently, the overall stochastic behavior of the element would be mesh-size dependent.

4. Numerical studies

The present model is applied to simulate the failure behavior of three-point and four-point bend specimens made of dense alumina ceramic. The loading configurations and geometries of the three-point and four-point bend specimens are shown in Fig. 7. For the three-point bend test, both notched and unnotched specimens are considered. For the notched beam, the initial notch depth is equal to 50% of the beam depth, and notch width is set to be $h_0/2$. To prevent localized damage and deformation near the loading and support points, elastic elements are used in these loading locations. The specimens are loaded in a displacement-controlled mode, which allows the entire load–deflection curve to be obtained. A sufficiently large number (approximately 400) of realizations are used to ensure convergence of both the mean peak load \bar{P}_m and the standard deviation of peak load δ_P , which are the two most important parameters for reliability-based structural design.

The random fields of elastic modulus E, tensile strength f_t , and fracture energy G_f are generated using the procedure described in Section 3.1. In this study, we consider that E and G_f follow a Gaussian distribution, and f_t follows the Gauss–Weibull distribution given by Bažant and Pang (2007), Bažant et al. (2009), Le et al. (2011), Bažant and Le (2017):

$$F_{f_t}(y) = \begin{cases} 1 - \exp\left[-(y/s_w)^{m_w}\right] & y \le y_g \\ P_g + \frac{r_g}{\delta_g \sqrt{2\pi}} \int_{y_g}^{y} \exp\left[-(y' - \mu_g)^2 / 2\delta_g^2\right] dy' & y > y_g \end{cases}$$
 (25)

where μ_g and δ_g are the mean and standard deviation, respectively, of the Gaussian core, m_w and s_w are the Weibull modulus and scaling parameter, respectively, of the Weibull tail, y_g and P_g are the grafting stress and grafting probability (i.e. $P_g = F_{f_i}(y_g)$),

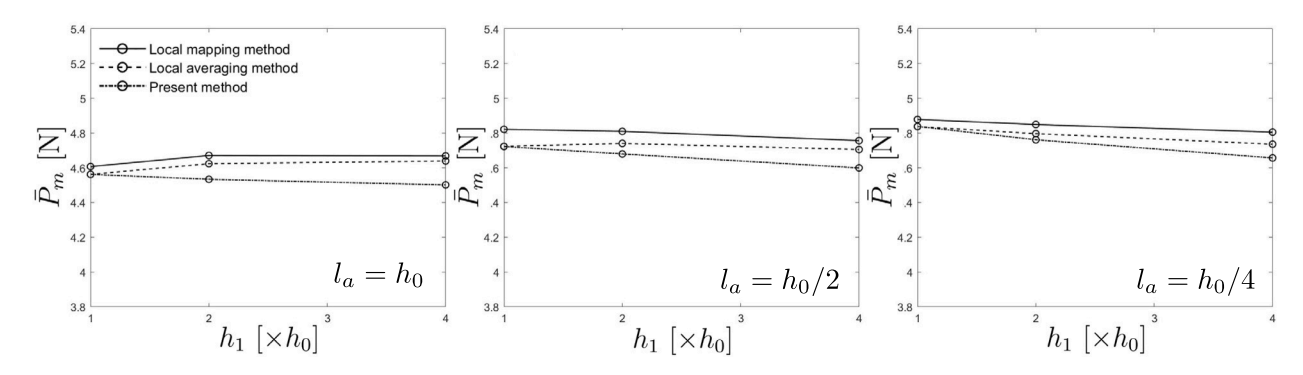


Fig. 8. Mean peak loads of unnotched three-point bend beam simulated using different mesh sizes and different CLs.

respectively, and r_g is a scaling parameter. The Gauss–Weibull cdf contains 6 parameters, among which four are independent. The remaining two parameters are determined by the continuity condition of the corresponding probability density function at the grafting point and the upper bound of F_{f_r} , i.e. $F_{f_r}(\infty) = 1$.

It should be mentioned that the elastic modulus and fracture energy would be better modeled also by the Gauss–Weibull distribution. However, it is expected that the Weibull tail of these two properties is too short to affect the sampling of the random values of E and G_f for the present analysis. By contrast, the Weibull tail of tensile strength is not very short, so it needs to be included for the sampling process.

For dense alumina ceramic, the following model parameters are used for the cdfs: the Young modulus E has a mean value $\mu_E=370$ GPa, and coefficient of variation (CoV) $\omega_E=0.15$; the fracture energy G_f has a mean value $\mu_{G_f}=50$ J/m² and CoV $\omega_{G_f}=0.15$; and for the tensile strength f_t we have $\mu_g=200$ MPa, $\delta_g=30$ MPa, $m_w=30$, and $P_g=5\times10^{-3}$. The Poisson ratio is taken as deterministic, $\nu=0.24$. The width of a single FPZ, h_0 is equal to 37.5 μ m, which is a few times the grain size.

In this study, the spatial variations of E, G_f , and f_i are characterized by squared exponential covariance functions (Grassl and Bažant, 2009; Le et al., 2018):

$$B_i(\tau) = \delta_i^2 \exp\left[-\left(\frac{\tau}{h}\right)^2\right] \tag{26}$$

where the subscript i=E, G_f , f_t denotes the Young modulus, fracture energy, and tensile strength, respectively, $\tau=$ distance between two points in the domain, δ_i is the standard deviation of the random material property i, and b is a scaling parameter. The scaling parameter b governs the correlation length (CL), l_a , of the random field. The CL is the minimum distance between two points where the random values of the material property can be practically considered as statistically independent. Here the CL is defined as $B_i(l_a)/\delta_i^2=0.1$, and therefore $b=l_a/\sqrt{\ln 10}$. To study the effect of CL on the mesh dependence of the stochastic FE analysis, we consider three different CL values: $l_a=h_0/4$, $h_0/2$, and h_0 .

The random fields $E(x_1, x_2)$, $G_f(x_1, x_2)$, and $f_t(x_1, x_2)$ are generated over the specimen domain with square grids of dimension $\Delta x \times \Delta x$ using the spectral representation method. In this study, we choose Δx to be $h_0/50$, which is sufficiently small to capture the spatial correlation of the random fields, as well as to avoid aliasing for the generation of the random fields.

The stochastic simulations are conducted in the open-source FEM software OOFEM with a Matlab interface for performing the mapping algorithm. The specimens are discretized into a structured mesh with 2D plane stress elements of an out-of-plane thickness h_0 . Each element has a height of h_0 . To investigate the mesh insensitivity, three different element widths $(h_0, 2h_0, \text{ and } 4h_0)$ are used in the simulation. As a comparative study on mesh sensitivity, we consider three mapping methods: (1) the present method, (2) local mapping method, in which the random constitutive property of the finite element is equal to the value of the random field of the corresponding material property at the centroid x_c of the finite element, i.e. $H_{FE}(x_c) = H(x_c)$, and (3) local averaging method, in which the random constitutive property of the finite element is equal to the average value of the random field of the corresponding material property over the domain of the finite element, i.e. $H_{FE}(x_c) = \frac{1}{A_c} \int_{\Omega_c} H(x) dA(x)$, where A_c area of the finite element. When comparing the proposed mapping method to the local mapping and local averaging methods, the same mechanism-based

When comparing the proposed mapping method to the local mapping and local averaging methods, the same mechanism-based energy regularization described by Section 2 is used for all simulation cases. This is to ensure that the observed mesh sensitivity, if any, is solely due to differences in mapping methods for the constitutive properties of the finite element. Following Gorgogianni et al. (2022), we choose $\chi_{t1} = 0$ and $\kappa = 1$ for energy regularization (Eq. (6)). The present model also involves parameter χ_{t2} for distinguishing between damage initiation and damage propagation. It is clear that χ_{t2} cannot be too large, otherwise the model would not be able to predict the propagation of localized damage if the mesh is not perfectly aligned in the propagation direction. On the other hand, if χ_{t2} is too small, the damage initiation would be inhibited. After several trial simulations, we choose $\chi_{t2} = 0.75 \chi_m$.

5. Results and discussion

Unnotched three-point bend beam

Fig. 8 presents the mean peak loads of the specimen simulated by using different mesh sizes and different CL values, l_a . It is seen that, for all CLs considered in this study, the mean peak loads \bar{P}_m predicted by using the aforementioned three mapping methods

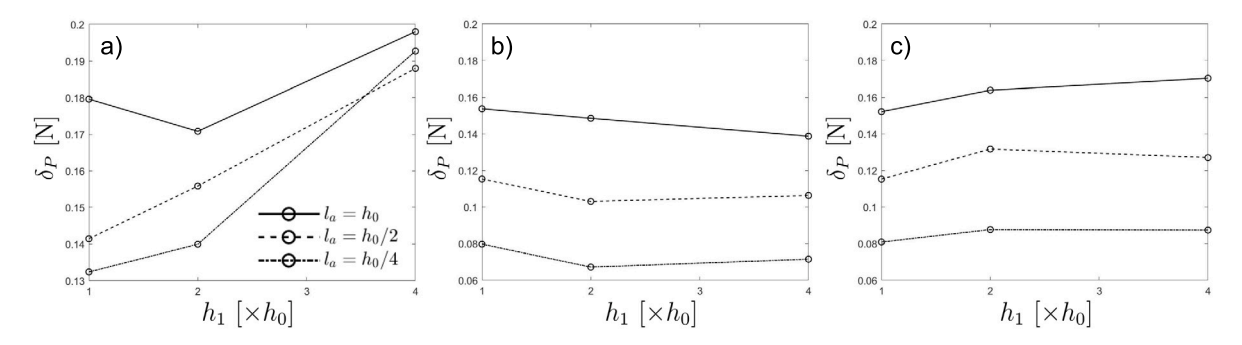


Fig. 9. Standard deviations of the peak load of unnotched three-point bend beam simulated using (a) local mapping method, (b) local averaging method, and (c) present method.



Fig. 10. Damage patterns of the unnotched three-point bend beam (zoom-in view of the damage zone) at (a) 95% pre-peak and (b) at the peak load.

are almost insensitive to the mesh size (the maximum difference in the predicted mean peak load is less than 2%). This is due to the present energy regularization scheme, which is used for all three mapping methods.

Fig. 9a presents the standard deviations, δ_P , of the peak load simulated by the local mapping method for different mesh sizes. It is seen that the standard deviation predicted by the local mapping method increases with the mesh size. This result can be explained from the damage pattern, as shown in Fig. 10. Upon loading, a damage zone of a considerable size is first formed at the mid-span region. At the peak load, a localized damage band forms and initiates from this damage zone. Upon continuing displacement-controlled loading, this localized damage band propagates in the form of a macrocrack. For a given l_a , the size of the initial damage zone is almost independent from the mesh size. Therefore, as the mesh size increases, there are fewer number of elements in the damage zone. Since the local mapping method uses the fixed cdfs of apparent tensile strength and fracture energy regardless of the mesh size, a decrease in the number of elements in the damage zone leads to an increasing variability in the energy dissipation of the damage zone. Furthermore, the initiation of a macrocrack at a random location inside the damage zone is behaviorally similar to a finite weakest-link model, where the number of elements in the chain corresponds to the number of elements in the damage zone. When mesh size increases, the number of elements in the chain decreases while the strength distribution of each element remains the same, thus also contributing to the larger variability in the peak load.

Fig. 9a also shows that, as the CL increases, the mesh dependence gets less pronounced. This is because, for a larger CL value, each finite element exhibits less spatial randomness of material property. Consequently, the statistics of constitutive properties of finite elements becomes less dependent on the element size. As long as a proper energy regularization scheme is implemented, the simulated mean and standard deviation of the peak load would exhibit less mesh dependence. Such a behavior is a general trend, which is also seen in the simulations of beams of other geometries for all three mapping methods.

Fig. 9b presents the results of δ_P simulated by using the local average method. It is seen that the local averaging method yields a less mesh-dependent response. This is because the local averaging method gives the correct mapping during the early loading stage, since the beam experiences a diffused damage pattern. As mentioned earlier, the initiation of localized damage inside one finite element exhibits a weakest-link feature as indicated by Eq. (21), which predicts that the statistical variation of apparent tensile strength should decrease with an increasing element size. On the other hand, the local averaging method also predicts such a behavior, however, due to the averaging effect (Vanmarcke, 2010). In general, the averaging effect predicts a larger decrease in the statistical variation with an increasing element size as compared to the weakest-link effect. Therefore, the local averaging method predicts that δ_P slightly decreases as the element size increases. Nevertheless, it should be pointed out that, even though the result of local average method does not exhibit strong mesh dependence, the method does not correspond to the correct damage pattern.

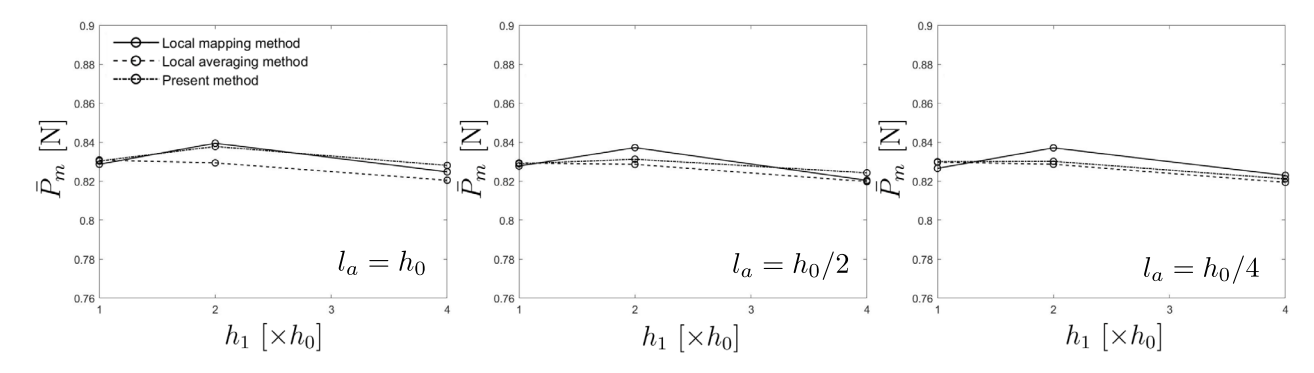


Fig. 11. Mean peak loads of notched three-point bend beam simulated using different mesh sizes and different CLs.

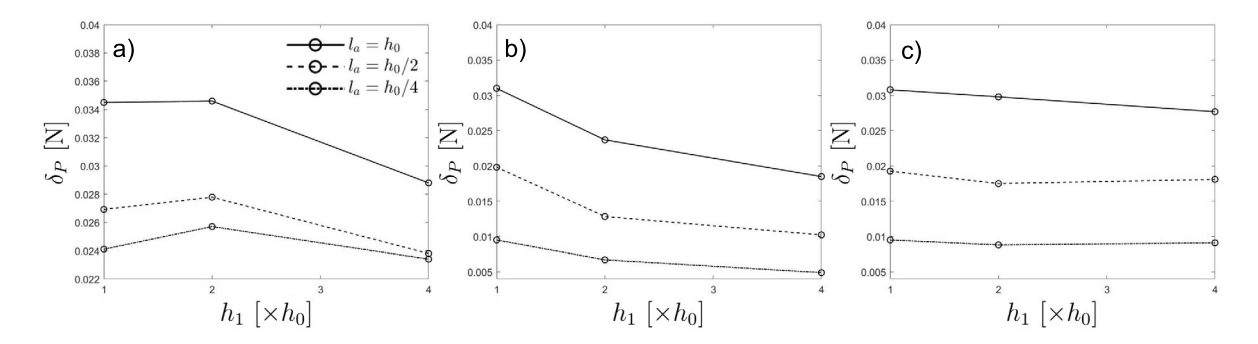


Fig. 12. Standard deviations of the peak load of notched three-point bend beam simulated using (a) local mapping method, (b) local averaging method, and (c) present method.

Fig. 9c presents the results of the present method. It is seen that the method yields a relatively mesh-insensitive standard deviation of peak load across all tested CL values. When the element size equals to h_0 , the present model is essentially the same as the local averaging method. As the element size increases, the present model shows a lesser degree of mesh dependence as compared to the local averaging method. It is seen that the present model predicts a higher value of δ_P than the local averaging method does. This is because, as mentioned before, the local averaging method underestimates the variability of apparent tensile strength at initiation of localized damage.

Notched three-point bend beam

Fig. 11 shows that, for all three methods, the simulated mean peak loads of the notched three-point bend beams are mesh insensitive. Due to stress concentration at the notch tip, localization occurs right after damage initiates, and therefore the energy regularization scheme essentially reduces to the crack band model (Bažant and Oh, 1983). The total energy dissipation for damage of the element is equal to the energy expended to propagate a single crack throughout the element. Such a localization behavior also dictates that the spatial randomness of material properties has no effects on the damage pattern. Therefore, the mean peak load is independent of the CL.

Fig. 12a presents the standard deviations of the peak load for different mesh sizes calculated by the local mapping method. In contrary to the case of unnotched three-point bend beams, the simulated δ_P of notched beam does not exhibit strong mesh dependence. Upon loading, the first element at the notch tip would experience a localized damage, whose location is determined by the notch tip. As the loading proceeds, the localized damage propagates upwards. At the peak load, several elements along the ligament are damaged. The important point here is that, due to damage propagation, the locations of the damage bands inside these elements are deterministic. The apparent tensile strength \widetilde{f}_t and fracture energy \widetilde{G}_f of the finite element are equal to the average tensile strength and fracture energy of one damage band. Consequently, the statistics of \widetilde{f}_t and \widetilde{G}_f are independent of the element size. Since the local mapping method does not calculate the average tensile strength and fracture energy of the band, it over-predicts the standard deviation of the peak load. Nevertheless, the model uses mesh-independent statistics of \widetilde{f}_t and \widetilde{G}_f , and therefore it is able to give a mesh-insensitive result regardless of the CL.

By contrast, the standard deviation δ_P calculated by the local averaging method exhibits a strong mesh dependence (Fig. 12b). For all three CLs, the calculated δ_P decreases significantly with an increasing mesh size. As mentioned earlier, the local averaging method predicts that the statistical variations of \widetilde{f}_t and \widetilde{G}_f decrease as the mesh size increases. However, the localized damage pattern of the notched beam dictates that the statistics of \widetilde{f}_t and \widetilde{G}_f should not be mesh dependent. This explains the mesh dependence of δ_P simulated by the local averaging method. By comparing the results for different CLs, it is seen that, when the element size increases

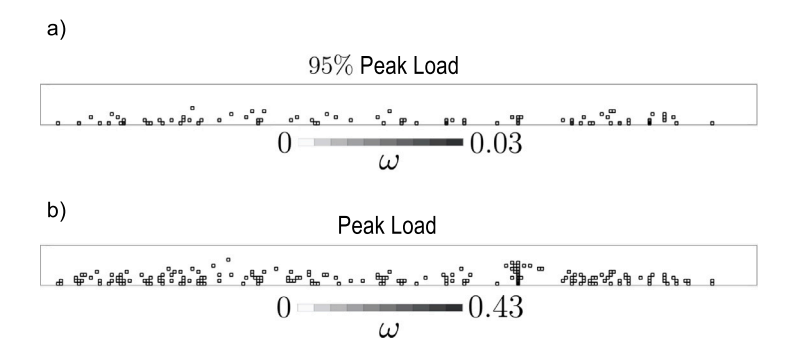


Fig. 13. Damage patterns of the unnotched four-point bend beam (zoom-in view of the damage zone) at (a) 95% pre-peak and (b) at the peak load.

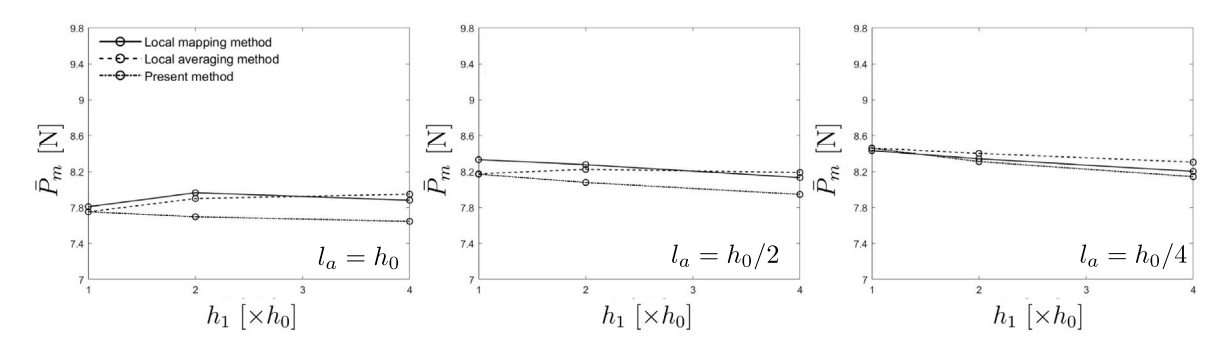


Fig. 14. Mean peak loads of unnotched four-point bend beam simulated using different mesh sizes and different CLs.

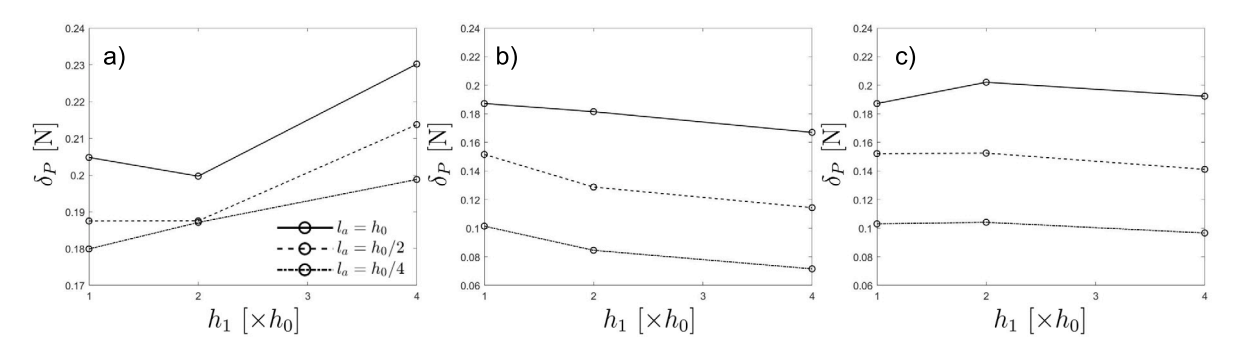


Fig. 15. Standard deviations of the peak load of unnotched four-point bend beam simulated using (a) local mapping method, (b) local averaging method, and (c) present method.

from h_0 to $4h_0$, the standard deviation δ_P decreases by almost 50% for $l_a = h_0/4$ while for $l_a = h_0$ the decrease in δ_P is less significant (about 33%).

As shown in Fig. 12c, the present method yields a nearly mesh-insensitive result of δ_P . In the simulation, parameter χ_2 of the elements along the ligament takes its maximum value as soon as damage occurs in the first element above the notch tip. The method samples the random values of \widetilde{f}_t and \widetilde{G}_f directly from the localized damage band, and therefore the resulting statistics of \widetilde{f}_t and \widetilde{G}_f are independent of the mesh size regardless of CL.

Unnotched four-point bend beam

The last numerical example is unnotched four-point bend beams. Since a large portion of the beam span experiences a constant moment in the elastic regime, the beam first exhibits a large distributed damage zone, and at the peak load several localized damage bands are formed at random locations inside the damage zone (Fig. 13). The simulation shows that, as compared to the localized damage band formed in the three-point bend beam, the damage level in these localized bands in four-point bend beams is higher, and therefore these localized damage bands play a more dominant role in determining the peak load.

Similar to the notched and unnotched three-point bend beams, the simulated mean peak loads of the four-point bend beam are mesh insensitive, as shown in Fig. 14. Fig. 15a shows that the standard deviation δ_P of the peak load simulated by the local

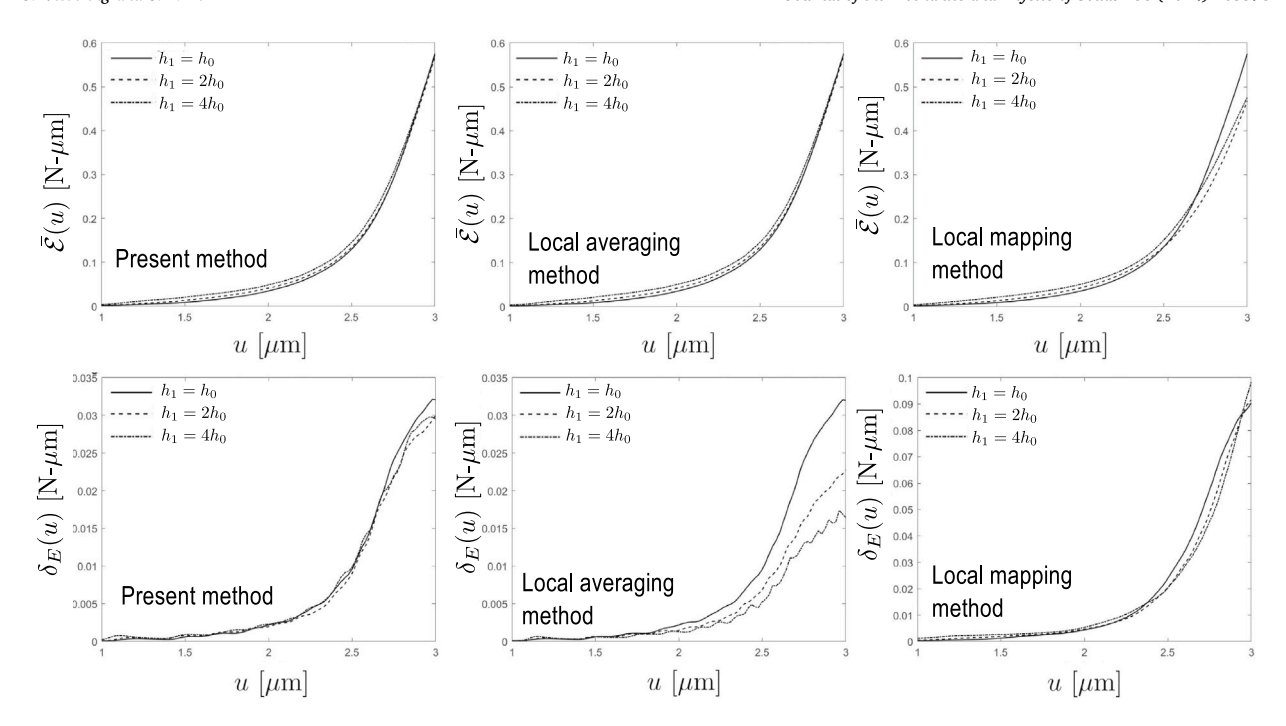


Fig. 16. Statistics of post-peak energy dissipation of notched three-point bend beam simulated using different projection methods (first row: mean behavior, and second row: standard deviation).

mapping method exhibits a strong mesh dependence. Similar to the simulation results of unnotched three-point bend beams, δ_P increases with an increasing mesh size. This mesh dependence arises from the fact that the local mapping method fails to capture the averaging effect of material properties for finite elements inside the distributed damage zone. On the other hand, it captures correctly that, during the propagation of localized damage, the statistics of \widetilde{f}_t and \widetilde{G}_f must be mesh independent. As mentioned before, the four-point bend beams contains several localized damage bands propagating from the initial damage zone, and the associated energy dissipations in these damage bands have considerable contributions to the peak load. Therefore, the mesh dependence of δ_P simulated by the local mapping method is less significant as compared to the case of unnotched three-point bend beams.

The foregoing discussion also explains the mesh dependence of δ_P simulated by the local averaging method shown in Fig. 15b. The method captures the averaging effect of random material properties for the distributed damage zone. However, it predicts incorrectly that the statistical variations of \widetilde{f}_t and \widetilde{G}_f decrease with an increasing mesh size for the propagation of localized damages, which has a major contribution to the peak load. Therefore, the local averaging method yields a more pronounced mesh dependence of δ_P for four-point bend beams as compared to unnotched three-point bend beams.

Compared to direct local mapping and direct local averaging method, the present method produces an almost mesh-sensitive result of δ_P for all three values of I_a (Fig. 15c). The method is capable of capturing the transition from a large diffused damage zone to the initiation and propagation of localized damage zones, as well as the corresponding change of the statistics of \widetilde{f}_t and \widetilde{G}_f during the transition.

Post-peak energy dissipation

The foregoing discussion focuses on the statistics of the peak load. It is also worthwhile to investigate the post-peak behavior of the beams. For all three loading configurations considered in this study, the post-peak behavior is featured by the propagation of localized macrocrack. Therefore, in this section we analyze the behavior of notched three-point bend beam, as a representative case. Here we are interested in the post-peak energy dissipation, which is calculated from the simulated load–deflection curve by

$$\mathcal{E}(u) = \int_0^u P(u') du' - \frac{1}{2} Pu \tag{27}$$

where P(u) = load-deflection curve. Since the constitutive model does not involve plasticity, $\mathcal{E}(u)$ represents the total energy dissipation due to damage at displacement u.

Fig. 16 presents the mean and standard deviations of $\mathcal{E}(u)$ for notched three-point bend beams for $l_a = h_0/4$. It is seen that the mean behaviors of $\mathcal{E}(u)$ simulated by all three methods are independent of the mesh size. With the energy regularization scheme, the mean energy dissipation expended for macrocrack propagation is guaranteed to be consistent with the fracture energy of the material. However, different mapping methods yield different levels of mesh dependence of the standard deviation of $\mathcal{E}(u)$, denoted by $\delta_E(u)$. The behavior of $\delta_E(u)$ predicted by the present model is nearly mesh independent. It is seen that δ_E increases with an increasing

displacement. This is because \mathcal{E} is equal to the total energy dissipation for propagating the macrocrack. Since the fracture energy is random along the ligament, the statistical variation of \mathcal{E} would increase as the applied displacement increases. It is worthwhile to comment on the slight mesh dependence observed in the behavior of $\delta_E(u)$. The simulation shows that this dependence arises from the mesh sensitivity of damage pattern. For large element size (element width $4h_0$), the macrocrack propagates vertically upwards. This is because, in the post-peak regime, the localization parameter $\delta_{\omega 2}$ of the elements along the ligament is larger than the threshold. Therefore, the newly formed damage band is perfectly aligned with the damage band in the elements below. For small element size (element width h_0), it is seen that the path of macrocrack propagation could be tortuous. The principal direction of the current element may not be horizontal. With a smaller element size, the projected crack path may not be perfectly vertical. Consequently, the variation of the energy dissipation for small elements is slightly higher than that for large elements.

The local averaging method gives a strong mesh-dependent result of $\delta_E(u)$. For any given displacement, $\delta_E(u)$ decreases with an increasing mesh size. This can be attributed to the fact that, by taking the average of random fracture energy, the variance of \widetilde{G}_f decreases considerably for large mesh size. As mentioned earlier, such an averaging procedure is inapplicable to the case of propagation of localized damage, in which the statistics of \widetilde{G}_f is set by the average fracture energy of one damage band. The result given by the local mapping method is almost mesh independent because, in this method, the statistics of \widetilde{G}_f is independent of the mesh size. However, the actual value of $\delta_E(u)$ predicted by the local mapping method is considerably higher than the prediction by the present method. This is because the local mapping method directly samples \widetilde{G}_f from the underlying random field of G_f without taking the average over the localized damage band.

6. Conclusions

Quasibrittle structures generally exhibit complex damage patterns and failure behaviors, which could involve both distributed and localized damage. These behaviors lead to intricate mesh dependence in stochastic FE simulations. It is shown that the energy regularization scheme is essential for mitigating the mesh dependence of the mean failure behavior, but is insufficient for addressing the mesh dependence of the second-order statistics of failure behavior. It is shown that the mesh sensitivity becomes milder when the correlation length of the random fields of material properties becomes large as compared to the FE mesh size.

To mitigate the spurious mesh sensitivity, the essential problem is how to project the continuous random fields of material properties onto the FE mesh. In this study, a mechanism-based mapping method is developed. The salient feature of the method is that, during the loading process, the mapping algorithm is updated based on the evolution of the damage pattern, and the statistics of the constitutive properties of the finite element would change accordingly. One important implication of the present mapping method is that the resulting statistics of constitutive properties of the finite element could vary with the mesh size, and this mesh dependence is governed by the damage pattern.

The numerical studies show that the commonly used local mapping and local averaging methods are unsatisfactory in terms of suppressing mesh dependence of the second statistical moments of failure loads. These methods correspond to some specific physical behaviors: the local averaging method is only applicable to the diffused damage pattern, whereas the local mapping method is in a qualitative sense applicable to the propagation of a localized damage band. It is demonstrated that these methods can deliver satisfactory results only when the prevailing damage pattern in the structure matches the physical behavior implied by these methods. Otherwise, they would lead to strong mesh sensitivity.

By contrast, the present model provides a robust means for mitigating the mesh dependence of the second statistical moments of failure loads for different structural geometries featuring different failure mechanisms. The success of the present model is hinged on the link between the damage pattern and the mapping of the random fields of material properties, which is a key consideration for stochastic FE simulations of quasibrittle fracture.

CRediT authorship contribution statement

Josh Vievering: Writing – review & editing, Writing – original draft, Software, Investigation, Formal analysis. **Jia-Liang Le:** Writing – review & editing, Writing – original draft, Supervision, Methodology, Investigation, Formal analysis, Conceptualization.

Declaration of competing interest

The authors declare the following financial interests/personal relationships which may be considered as potential competing interests: Jia-Liang Le reports financial support was provided by National Science Foundation. If there are other authors, they declare that they have no known competing financial interests or personal relationships that could have appeared to influence the work reported in this paper.

Data availability

Data will be made available on request.

Acknowledgments

The authors gratefully acknowledge funding support from the U.S. National Science Foundation (Grant CMMI-2151209) to the University of Minnesota.

References

Bažant, Z.P., 1976. Instability, ductility, and size effect in strain-softening concrete. J. Engrg. Mech. Div. ASCE 102, EM2, 331-344.

Bažant, Z.P., 1984. Imbricate continuum and progressive fracturing of concrete and geomaterials. Meccanica 19, 86-93.

Bazant, Z.P., Cedolin, L., 1979. Blunt crack band propagation in finite element analysis. J. Engrg. Mech. Div., ASCE 105, 297-315.

Bažant, Z.P., Le, J.-L., 2017. Probabilistic Mechanics of Quasibrittle Structures: Strength, Lifetime, and Size Effect. Cambridge University Press, Cambridge, U.K.. Bažant, Z.P., Le, J.-L., Bazant, M.Z., 2009. Scaling of strength and lifetime distributions of quasibrittle structures based on atomistic fracture mechanics. Proc. Natl. Acad. Sci. USA 106, 11484–11489.

Bažant, Z.P., Le, J.-L., Salviato, M., 2021. Quasibrittle Fracture Mechanics: A First Course. Oxford University Press, Oxford, U.K..

Bažant, Z.P., Oh, B.-H., 1983. Crack band theory for fracture of concrete. Mater. Struct. 16, 155-177.

Bazant, Z.P., Pang, S.D., 2006. Mechanics based statistics of failure risk of quasibrittle structures and size effect on safety factors. Proc. Natl. Acad. Sci. USA 103, 9434–9439.

Bažant, Z.P., Pang, S.D., 2007. Activation energy based extreme value statistics and size effect in brittle and quasibrittle fracture. J. Mech. Phys. Solids 55, 91–131.

Bažant, Z.P., Pijaudier-Cabot, G., 1988. Nonlocal continuum damage, localization instability and convergence. J. Appl. Mech. ASME 55, 287-293.

Bažant, Z.P., Planas, J., 1998. Fracture and Size Effect in Concrete and Other Quasibrittle Materials. CRC Press, Boca Raton, FL.

Bracewell, R.N., 1999. Fourier Transform and its Applications, third ed. McGraw-Hill.

Cervenka, J., Bazant, Z.P., Wierer, M., 2005. Equivalent localization element for crack band approach to mesh-sensitivity in microplane model. Int. J. Numer. Methods Engrg. 62, 700–726.

Deodatis, G., 1991. Weighted integral method I: stochastic stiffness matrix. J. Engrg. Mech. ASCE 117, 1851-1864.

der Kiureghian, A., Ke, J.B., 1988. The stochastic finite element method in structural reliability. Prob. Engrg. Mech. 3, 83-91.

Field, Jr., R., Grigoriu, M., 2012. A method for the efficient construction and sampling of vector-valued translation random fields. Prob. Eng. Mech. 29, 79–91. Ghanem, R., Spanos, P.D., 1991. Stochastic Finite Elements: A Spectral Approach. Springer-Verlag, Berlin.

Gorgogianni, A., Eliáš, J., Le, J.-L., 2020. Mechanism-based energy regularization in computational modeling of quasibrittle fracture. J. Appl. Mech. (ISSN: 0021-8936) 87 (9).

Gorgogianni, A., Elias, J., Le, J.-L., 2022. Mesh objective stochastic simulations of quasibrittle fracture. J. Mech. Phys. Solids 159, 104745.

Grassl, P., Bažant, Z.P., 2009. Random lattice-particle simulation of statistical size effect in quasi-brittle structures failing at crack initiation. J. Engrg. Mech., ASCE (ISSN: 0733-9399) 135 (2), 85–92. http://dx.doi.org/10.1061/(ASCE)0733-9399(2009)135:2(85).

Grigoriu, M., 1995. Applied Non-Gaussian Processes: Examples, Theory, Simulation, Linear Random Vibration, and Matlab Solutions. Prentice Hall, New Jersey. Haldar, A., Mahadevan, S., 2000. Reliability Assessment using Stochastic Finite Element Analysis. Wiley, New York.

Jirásek, M., Bauer, M., 2012. Numerical aspects of the crack band approach. Comput. Struct. 110-111, 60-78.

Kachanov, L., 1986. Introduction to Continuum Damage Mechanics. Springer, Netherlands.

Karhunen, K., 1946. Zur Spektraltheorie Stochastischer Prozesse. In: Suomalaisen Tiedeakatemian Toimituksia: Sarja A=Series A. 1, Mathematica, Physica; 34, Suomalainen Tiedeakatemia, Helsinki.

Le, J.-L., 2020. Level excursion analysis of probabilistic quasibrittle fracture. Sci. China: Tech. Sci. 63, 1141-1153.

Le, J.-L., Bažant, Z.P., Bazant, M.Z., 2011. Unified nano-mechanics based probabilistic theory of quasibrittle and brittle structures: I. Strength, crack growth, lifetime and scaling, J. Mech. Phys. Solids 59, 1291–1321.

Le, J.-L., Eliáš, J., 2016. A probabilistic crack band model for quasibrittle fracture. J. Appl. Mech. ASME 83 (5), 051005.

Le, J.-L., Eliáš, J., Gorgogianni, A., Vievering, J., Květon, J., 2018. Rate-dependent scaling of dynamic tensile strength of quasibrittle structures. J. Appl. Mech. (ISSN: 15289036) 85 (2), 021003. http://dx.doi.org/10.1115/1.4038496.

Luo, W., Bažant, Z.P., 2017. Fishnet statistics for probabilistic strength and scaling of nacreous imbricated lamellar materials. J. Mech. Phys. Solids 109, 264–287. Luo, W., Bažant, Z.P., 2019. Fishnet statistical size effect on strength of materials with nacreous microstructure. J. Appl. Mech. ASME (ISSN: 0021-8936) 86 (8). Mazars, J., 1984. Application de la Mécanique de l'Endommagement au Comportement non linéaire et à la Rupture du Béton de Structure (Ph.D. thesis). University of Paris VI, Paris, France.

Peerlings, R.H.J., de Borst, R., Brekelmans, W.A.M., de Vree, J.H.P., 1996. Gradient enhanced damage for quasi-brittle materials. Int. J. Numer. Methods Engrg. 39 (19), 3391–3403.

Pietruszczak, S., Mroz, Z., 1981. Finite element analysis of deformation of strain-softening materials. Int. J. Numer. Methods Engrg. 17, 327-334.

Sakamoto, S., Ghanem, R., 2002. Polynomial chaos decomposition for the simulation of non-Gaussian non-stationary stochastic processes. J. Engrg. Mech. ASCE 128, 190–201.

Shields, M.D., Deodatis, G., Bocchini, P., 2011. A simple and efficient methodology to approximate a general non-Gaussian stationary stochastic process by a translation process. Prob. Eng. Mech. 511–519.

Shinozuka, M., Deodatis, G., 1991. Simulation of stochastic processes by spectral representation. Appl. Mech. Rev. 44 (4), 191-204.

Shinozuka, M., Deodatis, G., 1996. Simulation of multi-dimensional Gaussian stochastic fields by spectral representation. Appl. Mech. Rev. 49 (1), 29-53.

Spanos, P.D., Ghanem, R.G., 1989. Stochastic finite element expansion for random media. J. Eng. Mech. ASCE 115 (5), 1035-1053.

Vanmarcke, E., 2010. Random Fields Analysis and Synthesis. World Scientific Publishers, Singapore.

Vanmarcke, E., Grigoriu, M., 1983. Stochastic finite element analysis of simple beams. J. Engrg. Mech. ASCE 109, 1203-1214.

Vio, R., Andreani, P., Tenorio, L., Wamsteker, W., 2002. Numerical simulation of non-Gaussian random fields with prescribed marginal distributions and cross-correlation structure. II. Multivariate random fields. Publ. Astron. Soc. Pac. 114 (801), 1281–1289.

Vořechovský, M., 2008. Simulation of simply cross correlated random fields by series expansion methods. Struct. Saf. 30 (4), 337-363.

Wu, J.-Y., Nguyen, V.P., 2018. A length scale insensitive phase-field damage model for brittle fracture. J. Mech. Phys. Solids 119, 20-42.

Wu, J.-Y., Yao, J.-R., Le, J.-L., 2023. Phase-field modeling of stochastic fracture in heterogeneous quasi-brittle solids. Comput. Methods Appl. Mech. Engrg. 416, 116332.

Xu, Z., Le, J.-L., 2017. A first passage model for probabilistic failure of polycrystalline silicon mems structures. J. Mech. Phys. Solids 99, 225-241.

Xu, H., Vievering, J., Nguyen, H.T., Zhang, Y., Le, J.-L., Bažant, Z.P., 2024. Asymptotically matched extrapolation of fishnet failure probability to continuum scale. J. Mech. Phys. Solids 182, 105479.

Yamazaki, F., Shinozuka, M., 1988. Digital generation of non-Gaussian stochastic fields. J. Eng. Mech. 114 (7), 1183-1197.